$M_{n+1}AX_n$ phases in the Ti-Si-C system studied by thin-film synthesis and *ab initio* calculations

J.-P. Palmquist,[1] S. Li,[2] P. O. Å. Persson,[3] J. Emmerlich,[3] O. Wilhelmsson,[1] H. Högberg,[3] M. I. Katsnelson,[2] B. Johansson,[2] R. Ahuja,[2] O. Eriksson,[2] L. Hultman,[3] and U. Jansson[1]

[1]*Uppsala University, Department of Materials Chemistry, The Ångström Laboratory, P.O. Box 538 SE-751 21 Uppsala, Sweden*

[2]*Uppsala University, Department of Physics, The Ångström Laboratory, P.O. Box 530 SE-751 21 Uppsala, Sweden*

[3]*Linköping University, Department of Physics, IFM, Thin Film Physics Division, SE-581 83 Linköping, Sweden*

(Received 3 November 2003; published 1 October 2004)

Thin films of $M_{n+1}AX_n$ layered compounds in the Ti-Si-C system were deposited on MgO(111) and Al_2O_3(0001) substrates held at 900 °C using dc magnetron sputtering from elemental targets of Ti, Si, and C. We report on single-crystal and epitaxial deposition of Ti_3SiC_2 (the previously reported *MAX* phase in the Ti-Si-C system), a previously unknown *MAX* phase Ti_4SiC_3 and another type of structure having the stoichiometry of $Ti_5Si_2C_3$ and $Ti_7Si_2C_5$. The latter two structures can be viewed as an intergrowth of 2 and 3 or 3 and 4 *M* layers between each *A* layer. In addition, epitaxial films of $Ti_5Si_3C_x$ were deposited and Ti_5Si_4 is also observed. First-principles calculations, based on density functional theory (DFT) of $Ti_{n+1}SiC_n$ for n=1,2,3,4 and the observed intergrown $Ti_5Si_2C_3$ and $Ti_7Si_2C_5$ structures show that the calculated difference in cohesive energy between the *MAX* phases reported here and competing phases (TiC, Ti_3SiC_2, $TiSi_2$, and Ti_5Si_3) are very small. This suggests that the observed $Ti_5Si_2C_3$ and $Ti_7Si_2C_5$ structures at least should be considered as metastable phases. The calculations show that the energy required for insertion of a Si layer in the TiC matrix is independent of how close the Si layers are stacked. Hardness and electrical properties can be related to the number of Si layers per Ti layer. This opens up for designed thin film structures the possibility to tune properties.

DOI: 10.1103/PhysRevB.70.165401 PACS number(s): 68.55.Nq, 81.15.Cd, 71.20.Be, 31.10.+z

I. INTRODUCTION

MAX-phases are a group of ternary and layered compounds with Ti_3SiC_2 as the most studied representative. The composition of these compounds can be written as $M_{n+1}AX_n$ (n=1–3) where *M* is an early transition metal, *A* is a *p* element, usually group IIIA and IVA and *X* is carbon or nitrogen.[1,2] Figure 1 shows the three different crystal structures that have been described in the literature M_2AX, M_3AX_2, and M_4AX_3, henceforth called 211, 312, and 413, respectively. These structures can be described as a nanolaminate with layers of a binary carbide or nitride *MX* interleaved with a single layer of *A* atoms. The insertion of *A* layers means that *M*-*A* bonds replace *M*-*X* bonds. The difference between, e.g., Ti_3SiC_2 and pure TiC is that single layers of interstitial C atoms have been exchanged with Si layers. In addition, the nanolaminate TiC layers on each side of the inserted Si layers are twinned with the Si layer as a mirror plane.[1,3,4] The major difference between the $M_{n+1}AX_n$, n=1,2,3, phases is the number of inserted *A* layers per *M* layer. This value can vary from, e.g., 0.5 *A*-layer/*M*-layer in the 211 phase to 0.25 *A* layer/*M*-layer in the 413 phase. It is likely that the stability and physical properties of different $M_{n+1}AX_n$ phases can be understood from a detailed study of the *M*-*A* and *M*-*X* interactions. It has been shown that *ab initio* calculations can be a useful approach to bring light on this topic, for example in Refs. 5 and 6.

The nanolayered structure of Ti_3SiC_2 with one Si layer for every three Ti layers gives this compound a combination of very interesting and useful characteristics.[7] It is reported to have refractory ceramic properties and yet be damage tolerant and withstand thermal shock in combination with good electrical and tribological properties.[8–13] It is also easily machinable and exhibits surface orientations with low friction and self-lubricating properties.[14,15] Figure 2 shows a ternary section of the Ti-Si-C system determined at 1100 °C by Wakelkamp *et al.*[16] The phase diagram suggests that the only stable $Ti_{n+1}SiC_n$ *MAX* phase is Ti_3SiC_2. Ti_3SiC_2 can be synthesized as bulk material using sintering[17] and as thin film materials by chemical vapor deposition[18] and magnetron sputtering.[19] We have in recent studies described three approaches to deposit single crystal and epitaxial films of

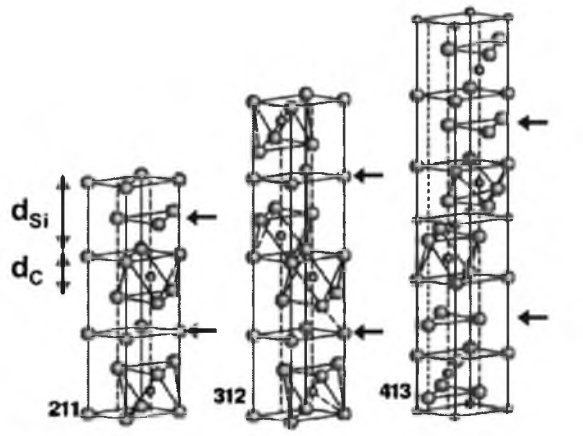

FIG. 1. (Color online) $M_{n+1}AX_n$ phase structures for n=1, 2, and 3 giving the three known subgroups referred to as 211, 312, and 413. Each structure shows one unit cell and the arrows show the Si layers. The *c* axis can be predicted in any given *MAX* structure by adding together the right number of Ti-Si-Ti and Ti-C-Ti distances, marked d_{Si} and d_C in the figure.

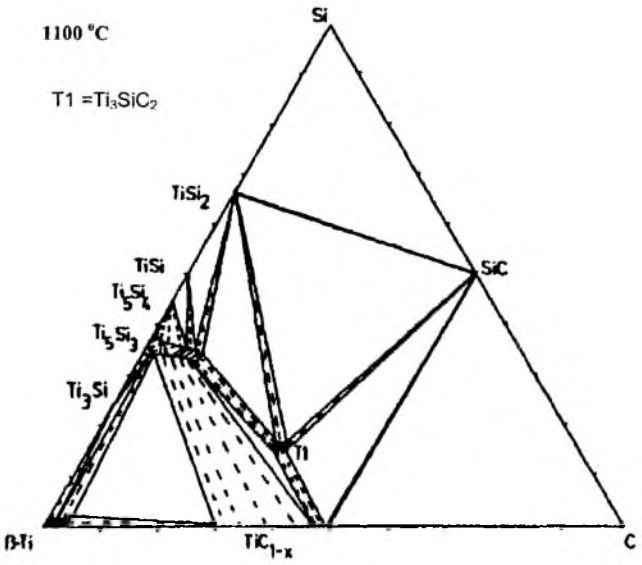

FIG. 2. The ternary phase diagram of Ti-Si-C determined at 1100 °C after Wakelkamp *et al.* (Ref. 16). T1 = Ti_3SiC_2.

Ti_3SiC_2 using (i) sputtering of Ti and Si with C_{60} as carbon source,[19,20] (ii) sputtering from a Ti_3SiC_2 compound target,[19,20] and (iii) unbalanced dc magnetron sputtering from individual Ti, Si, and C targets.[20,21] The *MAX* phases could be suitable for thin film applications such as, for example, low-friction gliding electrical contacts or as corrosive protecting coatings.

Considering the variety of $M_{n+1}AX_n$ phases for other transition metals, it is possible that other *MAX* phases can exist in the Ti-Si-C system, especially in the low-temperature regime where kinetic constraints can stabilize metastable phases. Such phases may exhibit properties similar, or perhaps, superior to Ti_3SiC_2. The main objective with this study is to make a systematic study of the phase formation in the Ti-Si-C system with a special emphasis to synthesize $Ti_{n+1}SiC_n$ *MAX* phases using thin film deposition. This means that we have concentrated our deposition experiments to films with 50 at % Ti and varied the Si and C contents. For this purpose, we employ dc magnetron sputtering from three targets, which offers the best control of the individual elemental fluxes.[21] Magnetron sputtering is also known to stabilize metastable phases since it is a synthesis technique that does not utilize thermodynamic equilibrium. The experimental study has been combined with theoretical *ab initio* calculations to achieve a better understanding of the phase stability in the $Ti_{n+1}SiC_n$ system. In particular, the effect of Si/Ti-layer ratio and its effect on stability and properties of the resulting $Ti_{n+1}SiC_n$ *MAX* phases are investigated.

II. EXPERIMENTAL SETUP

The Ti-Si-C films were deposited in an ultra high vacuum chamber (base pressure: 1×10^{-9} Torr) using unbalanced dc magnetron sputtering from three targets. Ti and C were sputtered from 3 in. targets and Si from a 1 in. target using 4 m Torr Ar pressure. The purity of the Ti, C, (pyrolytic graphite) and Si targets were 99.9, 99.9, and 99.999%, respectively. The individual fluxes of Ti, Si, and C were calibrated separately and controlled by the magnetron current. The Ti target was kept constant at 310 mA, while the Si and C targets were varied from 18 to 60 mA and 270 to 340 mA, respectively, which gave discharge voltages of, ~325, 450–500, and 510–550 V, respectively. The deposition rate was about 33 Å/min for the $Ti_{n+1}SiC_n$ films. Most films were deposited for 30 min giving ~1000 Å thick $Ti_{n+1}SiC_n$ films. Prior to deposition, the substrates, MgO(111), MgO(100), and Al_2O_3(0001) were degreased in trichloroethylene and isopropanole, thereafter preheated in the vacuum chamber to >800 °C for 1 h. The substrates were resistively heated from the backside and the temperature was monitored using a pyrometer.

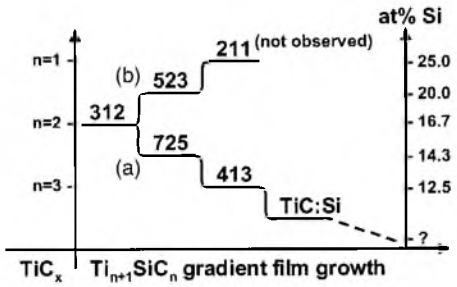

FIG. 3. Schematic sketch of how the multilayer films were deposited. Route (a) gives a film with lower Si content and route (b) films with higher Si content (note that the 211 phase was not observed within this study).

A 200-Å-thick TiC seed layer film was deposited for 8 min at 900 °C to aid the *MAX* film nucleation. During deposition there are two ways to initiate the $Ti_{n+1}SiC_n$ film growth: (i) The Si magnetron is started during the Ti-C deposition without interrupting the film growth. (ii) The TiC growth is interrupted using a shutter placed in front of the substrates while the Si magnetron is started. After a few minutes, when the magnetrons are stable, the shutter is removed and Ti-Si-C deposition is initiated. Both methods were tested and work equally well. To study the overall behavior of thin film growth in the $Ti_{n+1}SiC_n$ system multilayer *MAX* films were deposited such that the composition was changed every 1000 Å of growth. Figure 3 shows a schematic sketch of how this was carried out. The multilayer film deposition started with a stable 312 growth on TiC. Thereafter, the deposition fluxes were adjusted towards higher or lower Si content, in order to decrease or increase n in $Ti_{n+1}SiC_n$ (route *a* and *b*, respectively, in Fig. 3). Also, during this procedure the C content was adjusted correspondingly.

All films were characterized *ex situ* with x-ray diffraction (XRD). θ-2θ scans and ω scans [rocking curve (RC)] were recorded with a Siemens D5000 (Cu $K\alpha$ radiation) using an x-ray Göbel-mirror setup and a Soller slit on the detector. φ scans and reciprocal space maps (RSMs) were performed to characterize the epitaxial relationships. The chemical compositions of the films were studied with x-ray photoelectron spectroscopy (XPS) using a Phi Quantum 2000 instrument with monochromatizied Al $K\alpha$ radiation. XPS depth profiles were made with an argon ion sputter. A Ti_3SiC_2 standard (Kanthal AB, Sweden) was used to calculate sensitivity factors for the quantitative analysis.

TABLE I. Rocking curve full width at half maximum (RC FWHM) of epitaxial films on $Al_2O_3(0001)$ and MgO(111) substrates.

			Substrate	
			MgO(111)	$Al_2O_3(0001)$
n	Epitaxial film	Peak	RC FWHM[a](°)	RC FWHM[a](°)
Seed layer	TiC_x	(111)	1.3(1.8–2.0)	0.5(0.6–0.7)
1	Ti_2SiC			
2	Ti_3SiC_2	(0008)	0.85(1.3–2.0)	0.37(0.6–0.7)
3	Ti_4SiC_3	(000 10)	1.2(1.3–2.0)	0.6(0.7–0.8)
4	Ti_5SiC_4			
1.5	$Ti_5Si_2C_3$	(0004)		0.4
2.5	$Ti_7Si_2C_5$	(000 18)	1.2(1.3–2.0)	0.6
Silicide	$Ti_5Si_3C_x$	(0002)	0.8(1.2–2.0)	0.4(0.5–0.9)
Silicide	$Ti_5Si_4C_?$	(0002)	1.0(1.2–2.0)	0.7(1.2–2.0)

[a]Best observed FWHM and commonly observed FWHM in parenthesis.

The transmission electron microscopy (TEM) investigations were carried out using a JEOL 2010 FEG analytical STEM and a Philips CM 20 UT for high-resolution microscopy (HREM). A Technai 200 UT instrument was used for high-angle annular dark field (HAADF) in 1.4 Å probe scanning TEM mode imaging. Cross sectional samples were prepared using low-angle (4°) ion milling, in a Gatan PIPS operated at 5 kV. A final polishing stage using low-energy ions at 2 kV was applied to remove the amorphous surface layer formed in the previous stage.

Four-point-probe (Jandel, I=4.532 mA) was used to measure the sheet resistance R_S. The bulk resistivity ρ was calculated from the film thickness t:

$$R_S = 4.532\ (U/I) \text{ and } \rho = R_S\ t.$$

The TiC seed layer has been omitted when presenting the resistance data. The system can be viewed as two parallel-coupled resistors where the resistance in the TiC is about one order of magnitude larger than the *MAX*-phase film and also less than 20% of the total film thickness. This means that the TiC contribution to the total sheet resistance is more or less negligible. Hardness and Young's modulus were measured at room temperature on >0.5-μm-thick films with a Triboscope® (Hysitron, Inc.) using a three-sided pyramidal Berkovich indenter. The properties were calculated using the Oliver and Pharr method.[22] A series of six indents in the range of 100 to 3000 μN were made for every load. An atomic force microscope (AFM) imaging system was connected to the indentation system to display indents and plastic deformations around the indented surface as we report elsewhere.[23]

III. EXPERIMENTAL RESULTS

A. Epitaxial $Ti_{n+1}SiC_n$ growth on TiC(111) seed layer

The *MAX*-phase films in this study were deposited on a 200-Å-thick TiC seed layer on MgO(111) and $Al_2O_3(0001)$ to obtain reproducible nucleation conditions. The TiC composition was determined with XPS to $TiC_{0.7-0.8}$. MgO and TiC have a $B1$ structure with the nominal mismatch 2.5%. φ scans show epitaxial "cube-on-cube" growth between the two, i. e. TiC(111)//MgO(111) with TiC[1 $\bar{1}$0]//MgO[1 $\bar{1}$0] in-plane relationship. Although the mismatch between TiC(111) and $Al_2O_3(0001)$ is 11.2%, $Al_2O_3(0001)$ also proves to be a good template for epitaxial TiC(111) films and a TiC(111)//$Al_2O_3(0001)$ growth is observed with an in-plane relationship of TiC[1 $\bar{1}$0]//Al_2O_3[10 $\bar{1}$0] and TiC[$\bar{1}$10]//Al_2O_3[$\bar{2}$110]. Table I shows the rocking curve (RC) full width at half maximum (FWHM) values of the TiC seed layer films. As can be seen, the TiC(111) on $Al_2O_3(0001)$ has a typical FWHM value of 0.5°. In contrast, TiC(111) on MgO(111) exhibits considerably higher FWHM values of 1.3–2.0°. The TiC(111) surface is an excellent substrate for the $Ti_{n+1}SiC_n$ film growth[19–21] since the TiC layers in the $Ti_{n+1}SiC_n(001)$ basal plane is *de facto* a TiC(111) surface. All $Ti_{n+1}SiC_n$ films in this study were found to exhibit the same epitaxial out of plane oriented c-axis growth, i.e., $Ti_{n+1}SiC_n(0001)$//TiC(111) with the in-plane relationship $Ti_{n+1}SiC_n$[2 $\bar{1}$ $\bar{1}$0]//TiC[1 $\bar{1}$0].

B. Ti_3SiC_2

According to the phase diagram in Fig. 2, the only known thermodynamically stable *MAX* compound in the Ti-Si-C system is Ti_3SiC_2.[16] This phase was routinely deposited as thin films at 900 °C. Figure 4 shows the XRD patterns from $Ti_{n+1}SiC_n$ films of different composition deposited on MgO(111) and $Al_2O_3(0001)$ substrates with TiC(111) seed layer. Figure 4(a) shows the diffractogram of a single phase 312 film on MgO(111). With the exception of substrate and seed layer peaks only the Ti_3SiC_2 000l peaks can be seen. This epitaxial c-axis growth behavior, i.e., $Ti_3SiC_2(0001)$//TiC(111), was obtained also for $Al_2O_3(0001)$ substrates. The in-plane relationship was determined with φ scans and the TiC layers in the *MAX* film

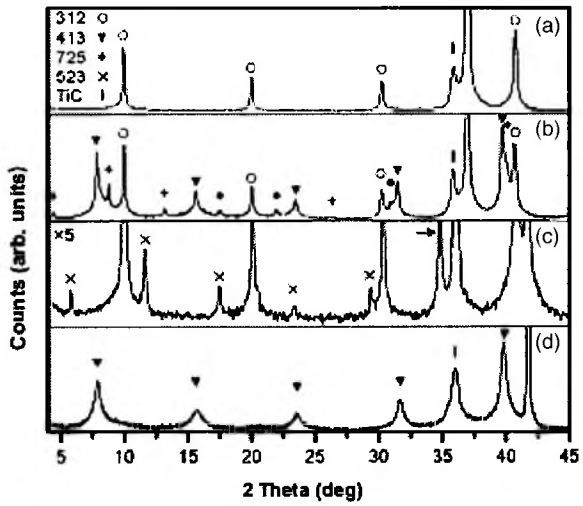

FIG. 4. X-ray diffraction (XRD) of $Ti_{1+n}SiC_n$ thin films from both single-phase films and multilayer films. (a) $Ti_3SiC_2(001)$ film deposited on TiC(111) seed layer on MgO(111) substrate. (b) $Ti_{1+n}SiC_n$ multilayer film deposited on TiC(111) seed-layer on MgO(111) following route (a) in Fig. 3 towards lower Si content. The triangles mark the Ti_4SiC_3 peaks. The (+) signs mark the peaks of a previously unknown type of *MAX*-phase structure $Ti_7Si_2C_5$, which can be viewed as an intergrowth of 312 and 413. (c) $Ti_{1+n}SiC_n$ multilayer film deposited on TiC(111) seed layer on $Al_2O_3(0001)$ following route (b) in Fig. 3. The (×) mark the peaks from the novel $Ti_5Si_2C_3$ phases, which can be described as an intergrowth of 211 and 312. (d) $Ti_4SiC_3(0001)$ film deposited on TiC(111) seed layer on $Al_2O_3(0001)$ substrate.

follow the orientation of the TiC(111) giving $Ti_3SiC_2[2\,\bar{1}\,\bar{1}0]//TiC[1\,\bar{1}0]$. The experimental unit cell parameters determined from the 312 films are presented in Table II. The *c* axis was calculated from the 000*l* peaks in the θ-2θ diffractogram and the *a* axis was determined with reciprocal space maps (RSM's) of $10\,\bar{1}\,l$ peaks (l=11 to 16). The intensity of the $\theta-2\theta$ XRD and RC indicates higher film crystal quality on $Al_2O_3(0001)$ substrates compared to

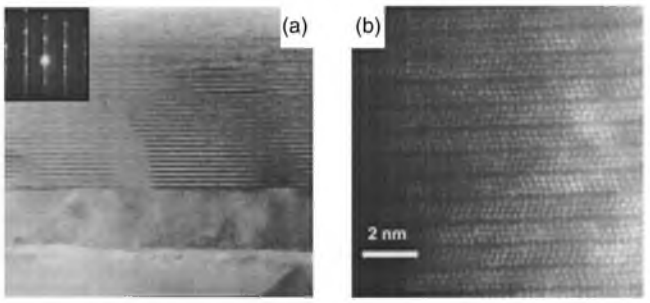

FIG. 5. (a) Cross-sectional TEM image of a $Ti_3SiC_2(0001)$ film on MgO(111) substrate with TiC(111) seed layer. The inset shows the corresponding selected area electron diffraction pattern. (b) HAADF image with atomic resolution, showing the layered structure of Ti_3SiC_2.

MgO(111). Table I shows that the RC FWHM of Ti_3SiC_2 are comparable to the FWHM of the TiC seed layer. Typical values for $Ti_3SiC_2(0008)$ on $Al_2O_3(0001)$ were in the range from 0.4° to 0.7° while films from the same experiment on MgO(111) were in the range of 1.3° to 2.0°.

Figure 5(a) shows a cross sectional TEM image of a 1000-Å-thick Ti_3SiC_2 film deposited on a ~200-Å-thick TiC(111) seed layer on MgO(111) substrate. The selected area electron diffraction pattern, inset in Fig. 5(a), shows the *c*-oriented *MAX*-phase film. Additional spots from the fcc lattice of the TiC and MgO substrate are also present. The HAADF image in Fig. 5(b) confirms that the material has the characteristic stacking sequence of the 312 structure. The bright spots represent the Ti atoms since the HAADF signal is atomic size dependent, lighter atoms show much less contrast. Thus, the dark horizontal lines make out the Si planes of the layered structure. The cross-sectional TEM analysis of all $Ti_3SiC_2(0001)$ films studied shows no grain boundaries over the analysed area in the microscope at magnifications down to 1000 times. Consequently, the $Ti_3SiC_2(001)$ films can be considered to be of single-crystal quality.

The stoichiometry of the Ti_3SiC_2films was measured with XPS. The analysis showed that the composition was close to

TABLE II. Unit cell parameters determined with XRD of thin films and DFT calculations. Predicted *c* axis from d_C and d_{Si} as indicated in Fig. 1.

		Measured		Calculated		Predicted[a]	
n	Phase	*a* axis (Å)	*c* axis (Å)	*a* axis (Å)	*c* axis (Å)	$d_C$and d_{Si}	*c* axis (Å)
Seed layer	TiC_x	4.325					
1	Ti_2SiC			3.01	12.67	$2d_C+2d_{Si}$	12.712
2	Ti_3SiC_2	3.06	17.65–17.77	3.03	17.45	$4d_C+2d_{Si}$	17.708
3	Ti_4SiC_3	3.05	22.67–22.73	3.03	22.31	$6d_C+2d_{Si}$	22.704
4	Ti_5SiC_4			3.04	27.24	$8d_C+2d_{Si}$	27.700
1.5	$Ti_5Si_2C_3$	3.06	30.42	2.99	30.38	$6d_C+4d_{Si}$	30.420
2.5	$Ti_7Si_2C_5$	3.06	40.37–40.45	3.06	40.18	$10d_C+4d_{Si}$	40.412
Silicide	$Ti_5Si_3C_x$		5.15–5.19			d_C	2.498
Silicide	$Ti_5Si_4C_x$?		12.74–12.77			d_{Si}	3.858

[a]$d_C=a_{TiC}/\sqrt{3}$ and d_{Si}=Ti-Si-Ti distance in Ti_3SiC_2.

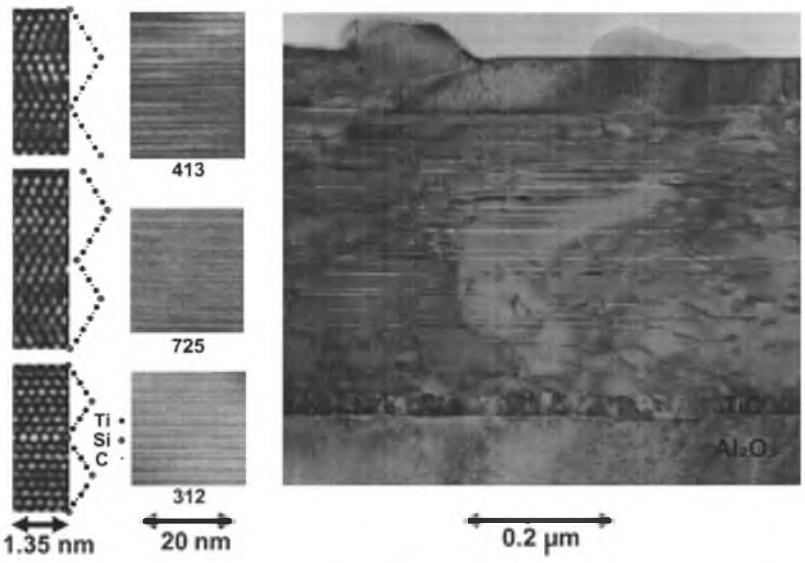

FIG. 6. The right image shows a cross-sectional TEM image of a multilayer film following route (a) in Fig. 3 towards lower Si content. Images of selected regions at medium magnification show 10 Si layers of the 312, 725, and 413 structure. To the left, the matched atom positions and stacking sequences are indicated schematically with each HREM inset, depending on the contrast conditions applied. The Si layers can be found as mirror planes in the stacking sequence.

3:1:2. However, variations of a few atomic percent could be observed in different samples, depending on the chosen element fluxes during film deposition. This supports the existence of a narrow homogeneity range in the Ti_3SiC_2 phase, as seen in the phase diagram in Fig. 2.[16]

C. Deposition of $Ti_{n+1}SiC_n$ multilayer films

Figure 4(b) shows an x-ray diffractogram of a multilayer film with compositional modulation according to route (a) in Fig. 3. The diffractogram shows a substrate MgO(111) peak at 36.9°, a seed-layer TiC(111) peak at 35.9°, and 312 *MAX* phase $Ti_3SiC_2(000l)$ peaks at 10.0°, 20.1°, 30.3°, and 40.8°, respectively. Furthermore, a series of peaks denoted with a triangle can be seen at 7.8°, 15.6°, 23.5°, 31.6°, and 39.7°. As will be shown below, these peaks can be attributed to the novel Ti_4SiC_3 *MAX* phase, with a *c* axis of ~22.7 Å. In addition, a number of other peaks can be seen at 4.4°, 8.7°, 13.1°, 17.5°, 22.0°, 26.4°, (30.9°, 35.5°), and 40.1° denoted with a plus (+) in Fig. 4(b). As will be discussed later, these peaks can be attributed to a previously unknown type of *MAX* phases. This phase has a unit cell *c* axis of ~40.4 Å, which is the sum of the 312 and the 413 *c*-axis. Therefore, in the following, we call this phase 725 (i.e., $Ti_7Si_2C_5$). Upon further reduction of the Si content, a $Ti_{n+1}SiC_n$ phase with n higher than 3 (i.e., Ti_5SiC_4, etc.) could not be observed by XRD. Instead, XPS and TEM detect a cubic TiC_x film (*B*1 structure) with a high concentration of Si.

Figure 6 contains a low magnification cross sectional image of a multilayer film following route (a) in Fig. 3. The Si content decreases during growth and subsequently with thickness. In the bottom of the image the Al_2O_3 substrate and the TiC bufferlayer can be seen. Each horizontal "line" in the image corresponds to the mirrorplane in the layered $Ti_{n+1}SiC_n$ *MAX* phases. Images of selected regions in the film show the different stacking sequences at medium magnification of 10 Si layers. These images are all 200 nm wide and the differences in stacking sequences govern the height of the image. For each sequence, the corresponding high-resolution image is shown to the left with a schematic. In the low magnification image, the near surface region contains low amounts of Si and the system prefers growth of a cubic TiC phase rather than the hexagonal $Ti_{n+1}SiC_n$ phase. However, still some occurrence of mirrorplanes can be seen and they become less frequent closer to the surface. This is in agreement with observations made by Yu *et al.* that report of Si-induced twinning of TiC accompanied with Si segregation to the twin boundaries, which leads to microtwins and formation of 2D Ti_3SiC_2 platelets.[24,25]

Figure 4(c) shows the diffractogram from a multilayer film where the Si content is increased (route *b* in Fig. 3). In addition to the peaks from the substrate, TiC and 312, several other peaks marked with a cross (×) can be observed at 5.81°, 11.62°, 17.48°, 23.37° and 29.33°. The peaks can be attributed to a previously unknown *MAX* phase with a *c* axis of ~30.4 Å. As for the 725 phase, the unit cell of this phase can be described as the sum of the 312 and 211 unit cells. In the following, this phase will be called 523 (i.e., $Ti_5Si_2C_3$). However, the 211 phase (Ti_2SiC) did not form in the multilayer films, nor in any other films. The arrow in Fig. 4(c) points at the $Ti_5Si_3C_x(0002)$ peak, a phase which was commonly observed in many films with high Si content. Formation of silicides and phase mixtures between silicides and *MAX* phases will be discussed in Sec. III F.

It should also be noted that other more random stacking sequences could be observed in some films. An example of this is given in the HAADF image in Fig. 7. The growth direction in the film is from right to left in the image. As can be seen, there are two broader regions with about ten "closed packed" layers of TiC between the interleaving Si layers. There can also be seen layers of three, four, and five TiC layers between each Si layer. Thereafter the film resumes the typical 312 stacking sequence.

D. Ti_4SiC_3

The *MAX* phase Ti_4SiC_3 could be deposited in multilayer films, as presented in Sec. III C, at reduced Si flux. The 413 has previously not been observed as bulk material in the Ti-Si-C system. This compound could be deposited as

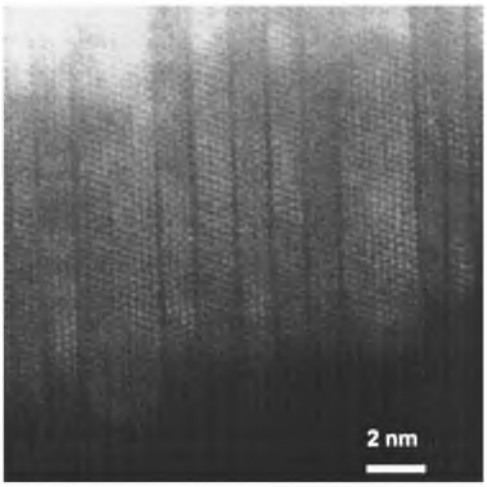

FIG. 7. TEM HAADF image of a *MAX*-phase film where the stacking sequence has been disturbed and each Si layer is separated with a random number of TiC layers.

single-phase films by a careful tuning of the deposition fluxes. Figure 4(d) shows the XRD pattern of a 2000 Å thick $Ti_4SiC_3(0001)$ film deposited on $TiC(111)//Al_2O_3(0001)$. Only the $000l$ peaks can be observed, i.e., the epitaxial growth is $Ti_4SiC_3(0001)//TiC(111)$ with an in-plane relationship $Ti_4SiC_3[10\bar{1}0]//TiC[1\bar{1}0]$. The typical stacking with four layers of Ti between the Si layers can be seen in the HREM image from the multilayer film, in Fig. 6. Small devations from Scherzer imaging conditions and difference in sample thickness between HREM insets in Fig. 6 influenced the contrast such as atom positions appears with dark contrast in 413 and 725, and bright contrast in 312 phase structures. It was also found that HREM imaging of these *MAX* phases were very sensitive to small deviations (mrad) from the exact zone axis, which resulted in apparent symmetry breaking of the lattice image. A slight imaging artifact can thus be seen in Fig. 6 and also in Fig. 8.

The experimental unit cell parameters for the 413 phase are shown in Table II. The c axis was determined from the $000l$ peaks and the a axis from RSM of $10\bar{1}l$ peaks (l=14 to 17). Variations in the c axis between different films were in the range of 0.1%, i.e., 22.70±0.03 Å. As for the Ti_3SiC_2 films, better crystalline quality was found on $Al_2O_3(001)$ substrates than on MgO(111). Table I shows RC FWHM values for the $Ti_4SiC_3(00010)$ peak in multilayer films on $Al_2O_3(0001)$ substrates in the range of 0.6° to 0.7° and on MgO(111) substrates between 1.3° to 2.0°.

E. $Ti_5Si_2C_3$ and $Ti_7Si_2C_5$: *MAX*-phase structures

The multilayer films presented in Sec. III C showed the existence of two previously unknown types of *MAX* phases $Ti_5Si_2C_3$ and $Ti_7Si_2C_5$. The 725 and 523 phases have yet not been deposited as single-phase films. They are generally observed as minority phases together with, e.g., Ti_3SiC_2 or, as already mentioned, in multilayer films. XRD evidently identifies them as well-ordered crystalline phases. If we assume the same hexagonal structure as the other *MAX* phases, the c axis can be determined from the $000l$ reflections ($l=2n$) in the $\theta-2\theta$ diffraction to 30.4 Å for $Ti_5Si_2C_3$ and 40.4 Å for $Ti_7Si_2C_5$, with small variations in different films, as presented in Table II. As can be seen in the HREM image in Fig. 8 the structure of 523 can be described as a combination of half-unit cells of 312 and half-unit cells of 211. It should be noted that observations of a pure Ti_2SiC phase has not been reported in literature. The stacking sequence of 523 during growth is alternating two and three Ti layers between each Si layer. In the same way the 725 phase has a structure which can be described as half cells of both phases 312 and 413, i.e., alternating three and four Ti layers between each Si layer. This can be seen in the HREM image of the 725 phase in Fig. 6. These observations correlate very well with the calculated c axis from the $000l$ reflections ($l=2n$) in $\theta-2\theta$ XRD. The c axis of 30.4 Å for 523 is equal to the sum of the observed c axis for 312 and the predicted c axis for 211. For the 725 the c axis is 40.4 Å, which is the sum of the observed 312 and 413 c axes.

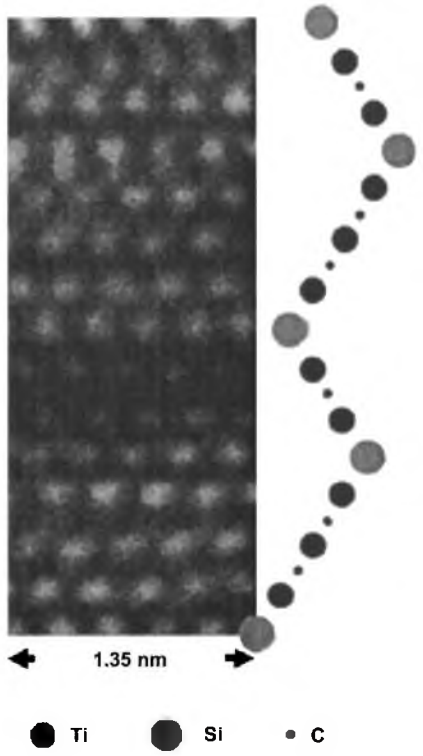

FIG. 8. Cross-sectional HREM image from a $Ti_{n+1}SiC_n$ film following route (a) in Fig. 3 showing the intergrown *MAX* phases $Ti_5Si_2C_3$, referred to as 523. The matched atom positions and stacking sequence are indicated schematically to the right. The Si layers can be found as mirror planes in the stacking sequence.

However, it should be observed that this description of the c axis cannot correctly reproduce the stacking sequence of the 523 and 725 phases. The alternating stacking of even and odd numbers of Ti layers induces a translation of the Si position in the lattice. This can be seen in the schematic atomic positions for 523 and 725, Figs. 8 and 6, respectively, where the Si atoms not are positioned on top of each other. That would require three repetitions instead of two. This suggests that the symmetry of the hexagonal space group D_{6h}^4

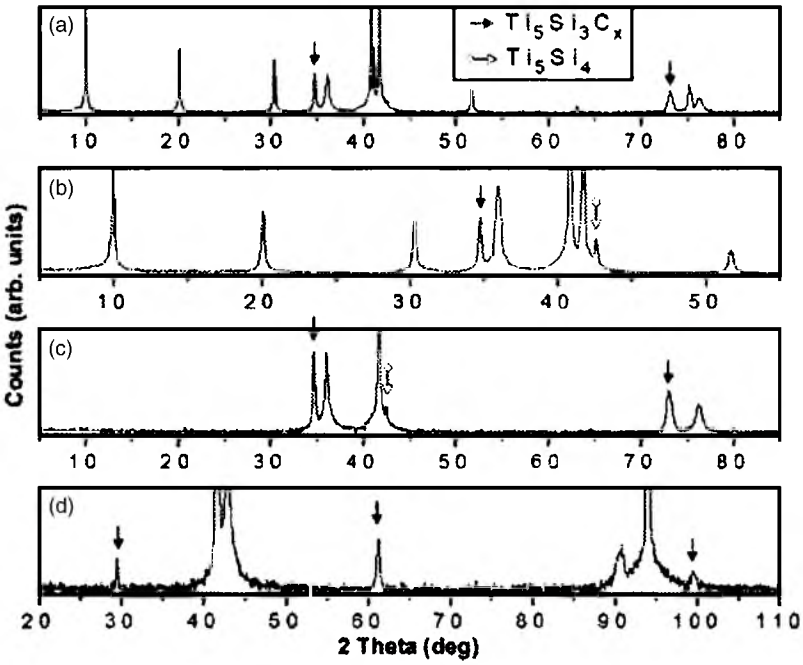

FIG. 9. θ-2θ diffractograms showing (a) Ti_3SiC_2 film on TiC-seed layer with the commonly observed impurity phase $Ti_5Si_3C_x$, which grows epitaxially with a c axis orientation. (b) Ti_3SiC_2 film on TiC-seed layer with both $Ti_5Si_3C_x$ and Ti_5Si_4 as impurity phases. (c) Epitaxially grown $Ti_5Si_3C_x(001)$ film on TiC(111) seed layer. (d) Epitaxially grown $Ti_5Si_3C_x(111)$ film on TiC(100) seed layer.

$-P6_3/mmc$, used for the *MAX* phases, is broken. However, the diffraction pattern from these intergrown structures could instead be indexed based on a hexagonal lattice with a c axis that is 1.5 times the basic hexagonal c axis, i.e., 45.63 and 60.62 Å for 523 and 725, respectively. In such a structure, the observed $000l$ reflections in the θ-2θ diffractogram would be indexed with $l=3n$. However, further studies are needed to settle this topic.

The a axis was determined from asymmetric peaks $(10\,\bar{1}\,l)$ using reciprocal space mapping (RSM). However, the a axis can only be estimated to be ~3.06 Å (=a axis of Ti_3SiC_2) since there are overlapping peaks from Ti_3SiC_2, which makes the maps hard to interpret (there is also the question regarding indexing, depending on what c axis is used). In conformity with the other $Ti_{n+1}SiC_n$ phases, the in-plane orientation of both $Ti_5Si_2C_3$ and $Ti_7Si_2C_5$ are $Ti_5Si_2C_3[2\,\bar{1}\,\bar{1}0]//Ti_3SiC_2[[2\,\bar{1}\,\bar{1}0]//TiC[1\,\bar{1}0]$ and $Ti_7Si_2C_5[[2\,\bar{1}\,\bar{1}0]//Ti_3SiC_2[[2\,\bar{1}\,\bar{1}0]//TiC[1\,\bar{1}0]$, respectively. Rocking curve of 523 and 725 phases reveals the same growth direction as the TiC(111) and the other $Ti_{n+1}SiC_n$ phases. Best observed RC FWHM values on $Al_2O_3(0001)$ substrate were 0.4° and 0.6° for $Ti_5Si_2C_3(0004)$ and $Ti_7Si_2C_5(00018)$, respectively. As with the other *MAX* films the RC FWHM is slightly higher on MgO(111) substrates. Finally, the RSM showed no indications of strain in the films.

F. Observations and epitaxial growth of silicide phases

The phase diagram of Ti-Si-C in Fig. 2 shows one ternary compound in addition to Ti_3SiC_2, namely, $Ti_5Si_3C_x$.[16] This phase can be considered as a solid solution of carbon into the binary silicide Ti_5Si_3.[26] In our study, $Ti_5Si_3C_x$ was observed as a minority phase in many films. The θ–2θ diffractogram in Fig. 9(a) shows a typical Ti_3SiC_2 film with a small, but easily identified silicide impurity. The phase diagram in Fig. 2 shows that there exists large homogeneity areas connected by two-phase regions.[16] Most deposited films containing the $Ti_5Si_3C_x$ phase have a composition within the two-phase area so it is not surprising that it can be formed. Rocking curves showed that this phase also exhibits an epitaxial growth with the same c axis orientation as the *MAX* films. The $Ti_5Si_3C_x$ has a hexagonal unit cell and XRD gives a c axis of 5.18 Å (with observed values in different films ranging from 5.16 to 5.20 Å). In films with higher Si content the XRD analysis shows that the silicide formation becomes more prominent and Ti_5Si_4 (or maybe $Ti_5Si_4C_x$) can also be identified, see Fig. 9 diffractogram (b).

Even though the silicide phases most often were observed in phase mixtures, it was also possible to deposit single phase epitaxial $Ti_5Si_3C_x(000l)$ films on the TiC(111) seed layer on $Al_2O_3(0001)$ as shown in Fig. 9 diffractogram (c). Rocking curves of the $Ti_5Si_3C_x(0002)$ peak showed a FWHM of 0.7°, but a lower RC FWHM of ~0.4°–0.5° was often seen in films consisting of phase mixtures. Phi scans showed a twinned growth where the in-plane relationship is $Ti_5Si_3C_x[110]$/(rotated ±9.5° around [110])/$TiC[1\,\bar{1}0]$. Furthermore, epitaxial $Ti_5Si_3C_x(111)$ films was grown on TiC(100) seed layer on MgO(100) substrate, see Fig. 9(d). The RC showed two domains (growth directions) separated by 0.5° and a $Ti_5Si_3C_x(222)$ RC FWHM of ~1°. Phi scans showed that the in-plane relationship is $Ti_5Si_3C_x[110]//TiC[100]//MgO[100]$.

G. Physical properties of the *MAX* films

Four point probe measurements were performed at room temperature on the films to determine the electrical conductance. Bulk resistivity was calculated from the sheet resistivity and the estimated film thickness. The results are presented in Table III. The resistivity of the $Ti_{n+1}SiC_n$ films is generally

TABLE III. Measured resistivity and calculated bulk modulus of the *MAX* phases in the Ti-Si-C system.

n	Phase	Experimental resistivity ($\mu\Omega$cm)	Calculated bulk modulus (GPa)
Seed layer	TiC_x	200–260	289
1	Ti_2SiC		205
2	Ti_3SiC_2	25–30	233
3	Ti_4SiC_3	50	245
4	Ti_5SiC_4		254
1.5	$Ti_5Si_2C_3$		224
2.5	$Ti_7Si_2C_5$		239
gradient film	312/523	30	
gradient film	312/725/413	27–40	
Silicide	$Ti_5Si_3C_x$	120–160	

very low. Single crystal $Ti_3SiC_2(000l)$ films have a resistivity of 25–30 $\mu\Omega$ cm. Single-phase films of $Ti_4SiC_3(0001)$ have a resistivity of about 50 $\mu\Omega$ cm. Epitaxial $TiCx(111)$, $x=0.7-0.8$, films grown under equivalent conditions have a resistivity in the range of 200 to 260 $\mu\Omega$ cm. Interestingly, the multilayer films of different *MAX* phases also had very low resistivity values in the range of 30 to 50 $\mu\Omega$ cm. However, incorporation of silicides in the *MAX* films has a negative effect on the conductance. Phase mixtures of Ti_3SiC_2 with $Ti_5Si_3C_x$ and Ti_5Si_4, gave resistivity values in the range of 40–80 $\mu\Omega$ cm. The epitaxial films of $Ti_5Si_3C_x$ (with or without Ti_5Si_4) had resistivity values of 140 to 160 $\mu\Omega$ cm. In general, we can conclude that all films containing 312 and other *MAX* phases exhibit a very good conducting behavior of almost an order of magnitude better than corresponding TiC_x films.

Hardness and Young's modulus have been measured on films deposited to a thickness of at least 0.5 μm. Nanoindentation in with a Berkovich indenter yielded hardness values of approximately 24 GPa for very small loads. Higher loads give lower hardness values due to the special deformation behavior of the *MAX* phases, as presented elsewhere.[23,27] The Young's modulus of the Ti_3SiC_2 films was approximately 340 GPa. No other single-phase films with a thickness of >0.5 μm were made in this study, therefore we cannot report hardness values for the 413, 523, or 725 phases. However, the observed hardness in gradient and multilayer films consisting of phase mixtures of 312, 413, and 725 phases in different proportions was within the error for a pure 312 film.

IV. THEORETICAL STUDY

A. Method

The experimental observation of previously unreported *MAX* phases in the Ti-Si-C system makes it very interesting to perform theoretical calculations on these compounds. We have used the Vienna *ab initio* simulation package (VASP) and projector augmented wave[28] (PAW) method as supplied by Kresse and Joubert.[29] The calculations of optimized geometries and total energy were performed within the local density approximation (LDA) based on the density functional theory (DFT). We used the Ceperley-Alder[30] exchange and correlation functional parameterized by Perdew and Zunger.[31] High-precision calculations with a cutoff energy of 500 eV for the plane-wave basis were performed. The Brillouin zone integration was carried out using the special **k**-point sampling of the Monkhorst-Pack type.[32] The total energies were converged to below 0.001 eV as regards the number of **k** points. The tetrahedron method with Blöchl corrections[33] was applied for both geometry relaxation and total energy calculations. The geometry optimization was considered to be convergenced when the total force on the atoms was less than 1×10^{-3} eV/Å, however, for bigger system, e.g., 725 it was around 1×10^{-2} eV/Å. All calculations have been carried out on stoichiometric phases without consideration to homogeneity ranges (e.g., TiC_x, $x=1$ and $Ti_5Si_3C_x$, $x=0$). For more detailed data about the calculations we refer to Li *et al.*[34] The phase stability has been predicted by comparing the total energy of the *MAX* phase with the total energy of the competing equilibrium phases at corresponding composition as given by the phase diagram in Fig. 2. Since the difference between the total energy and the cohesive energy of a phase only involves the total energy of the atomic form of the elements that build up a phase, one can for the purpose of evaluation phase stability (energy differences between different phases) use these two energies synonymously. We will use the cohesive energy, E_{coh} in our discussions.

B. Calculation of unit cell parameters

All *MAX* phases follow the general formula $M_{n+1}AX_n$ with a layered hexagonal structure that belongs to space group $D_{6h}^4-P6_3/mmc$. The value of $n=1,2,3$ gives the three reported crystal structures 211, 312, and 413, characterized by 2, 3, and 4 *MX* layers separating each *A* layer, respectively (see Fig. 1).[1] Table II shows the observed unit cell parameters for Ti_3SiC_2, Ti_4SiC_3, $Ti_5Si_2C_3$, and $Ti_7Si_2C_5$ together with the theoretical unit cell parameters obtained from our first principles calculations. Furthermore, calculated data for Ti_2SiC and Ti_5SiC_4 are included to complement the study. In addition, the *c* axis for a given *MAX* phase unit cell can also be predicted from the knowledge of the *M-X-M* and *M-A-M* distance, denoted d_C and d_{Si}, respectively in Fig. 1.[1] For comparison, Table II also present the predicted *c* axis for $Ti_{n+1}SiC_n$ structures ($n=1-4$) and for the novel $Ti_5Si_2C_3$ and $Ti_7Si_2C_5$ phases, using $d_C=a_{TiC}/\sqrt{3}$ and d_{Si} values from the Ti-Si-Ti distance in the 312 compound.[1]

The measured, calculated and predicted cell parameters have been used to calculate the volume of the unit cell per atom. As can be seen in Fig. 10(a), the volume increases linearly with the number of inserted Si layers per Ti layer. A small but noticeable trend of shorter *a* and *c* axes for the calculated cell data, leads to a smaller calculated volume/atom than measured. This slight tendency for overbinding is a well-known effect of the local density approximation.

C. Calculation of total energies and bulk modulus

The phase diagram in Fig. 2 shows that the competing phases for Ti_4SiC_3, Ti_5SiC_4, and $Ti_7Si_2C_5$ are Ti_3SiC_2 and

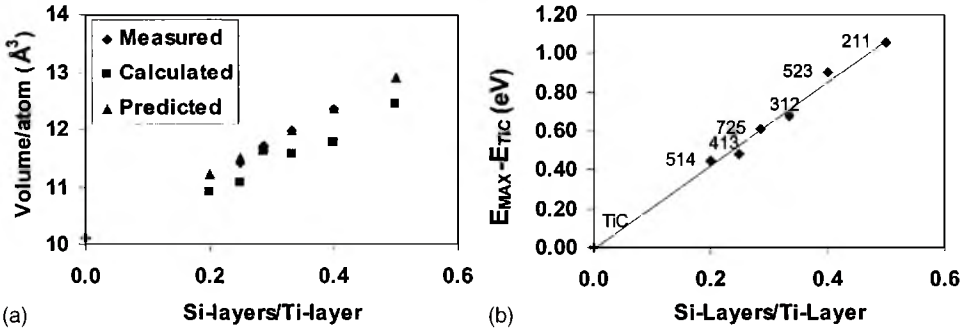

FIG. 10. (a) Volume per atom and (b) differences in cohesive energy between the $Ti_{n+1}SiC_n$ phases and TiC, plotted as a function of Si layers per Ti layer.

TiC, while the competing phases for Ti_2SiC and $Ti_5Si_2C_3$ are Ti_3SiC_2, $TiSi_2$, and Ti_5Si_3 (where the last also could be $Ti_5Si_3C_x$). It has been assumed that the phase diagram in Fig. 2 also is valid at 0 K. Table IV list the cohesive energy per atom (E_{coh}) for each of the calculated *MAX* phases and for the competing equilibrium phases. The stability of a given *MAX* phase is determined by the energy difference (ΔE) between the *MAX* phase and its competing phases. A negative ΔE indicates a stable phase. A positive ΔE suggests that it will decompose or not be formed at all in favour for the competing phases.

From Table IV, it can be seen that there is a very small, but negative, energy difference of -0.008 eV/atom, between the 211 phase and its competing phases. This suggests that the 211 could be stable, but it should be noted that the calculated energy difference is so small that it is approaching the accuracy of the calculations. A more significant negative energy difference is calculated for the 413 compound with −0.029 eV/atom. This suggests that the 413 phase actually is stable. For the 514 compound, the calculated energy difference is clearly positive, +0.037 eV/atom and this phase should therefore not be stable. The calculations of the *MAX* phase structures 523 and 725 show that the energy difference is positive compared with the competing phases; +0.036 eV/atom for the 523 compound and +0.030 eV/atom for the 725 compound. This suggests that both the observed intergrown phases should not be stable in bulk form.

It seems clear from Table IV that the cohesive energy of the $Ti_{n+1}SiC_n$ phases is dependent on the value of n. With increasing values of n the *MAX* phase becomes more similar to pure TiC and the number of Si layers per Ti layer is reduced. The extra energy, required to insert Si layers, can therefore be deduced by calculating the difference in cohesive energy between the $Ti_{n+1}SiC_n$ phases and pure TiC. In Fig. 10(b) this energy difference has been plotted as a function of the number of Si layers per Ti layer. Note from the figure that the energy difference increases (almost) linearly with the amount of Si layers per Ti layers in the structure. This is consistent with Ti-Si bonds being weaker than Ti-C bonds and that the Ti-Si and Ti-C bonds are constant in strength for all stoichiometries.

Our calculations of the bulk modulus (Table III) show that the Si layers in the Ti-Si-C system make the compound softer. The bulk modulus decreases with increasing number of Si layer per Ti layer, as seen by comparing Ti_2SiC to Ti_5SiC_4. The 523 phase is a combination of 211 and 312 and has a Si concentration intermediate of 211 and 312, hence it should have a bulk modulus higher than 211, but lower than 312. A calculated bulk modulus of 224 GPa is consistent with this analysis. All the studied Ti-Si-C compounds have a lower calculated bulk modulus compared to TiC. As shown in Fig. 11, the general trend of the bulk modulus can be clearly seen from our calculations; it decreases with increasing content of Si, although the bulk modulus is somewhat overestimated within the LDA approximation.

D. Electronic structure

The density of states (DOS) for all our calculated *MAX* phases and TiC are shown in Fig. 12. The lowest lying states,

TABLE IV. Calculated cohesive energy E_{coh} and difference in cohesive energy between the $Ti_{n+1}SiC_n$ phases and pure TiC, E_{tot}-E_{TiC}. Competing phases for Ti_2SiC, Ti_4SiC_3, Ti_5SiC_4, $Ti_5Si_2C_3$ and $Ti_7Si_2C_5$ and energy difference ΔE between these compounds and their assumed decompositional products. $\Delta E>0$ shows that the phase should not be stable, $\Delta E<0$ suggest that the phase is stable at 0 K.

n	Si-layer/ Ti-layer	Phase	E_{coh} (eV/atom)	E_{max}-E_{TiC} (eV/atom)	Competing phases[a]				ΔE (eV/atom)
	0	TiC	−10.1965	0					
1	0.5	Ti_2SiC	−9.1425	1.054	0.75	Ti_3SiC_2+0.107	$TiSi_2$+0.143	Ti_5Si_3	−0.008
2	0.33	Ti_3SiC_2	−9.5215	0.675					
3	0.25	Ti_4SiC_3	−9.7190	0.478	0.75	Ti_3SiC_2+0.25	TiC		−0.029
4	0.2	Ti_5SiC_4	−9.7542	0.442	0.6	Ti_3SiC_2+0.4	TiC		0.037
1.5	0.4	$Ti_5Si_2C_3$	−9.3309	0.866	0.9	Ti_3SiC_2+0.043	$TiSi_2$+0.057	Ti_5Si_3	0.036
2.5	0.286	$Ti_7Si_2C_5$	−9.5902	0.606	0.857	Ti_3SiC_2+0.143	TiC		0.028
		$TiSi_2$	−7.4287						
		Ti_5Si_3	−8.3846						

[a]As concluded from the phase diagram in Fig. 2.

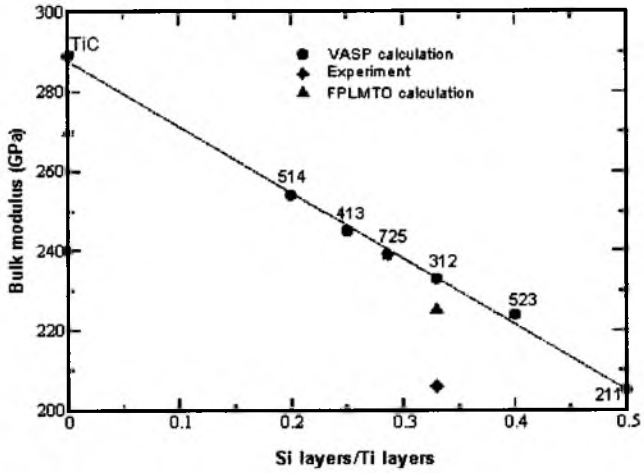

FIG. 11. (Color online) The calculated bulk modulus (B) for TiC, Ti_5SiC_4, Ti_4SiC_3, $Ti_7Si_2C_5$, Ti_3SiC_2, $Ti_5Si_2C_3$, and Ti_2SiC as a function of Si layers per Ti layer compared with literature data for TiC and Ti_3SiC_2.

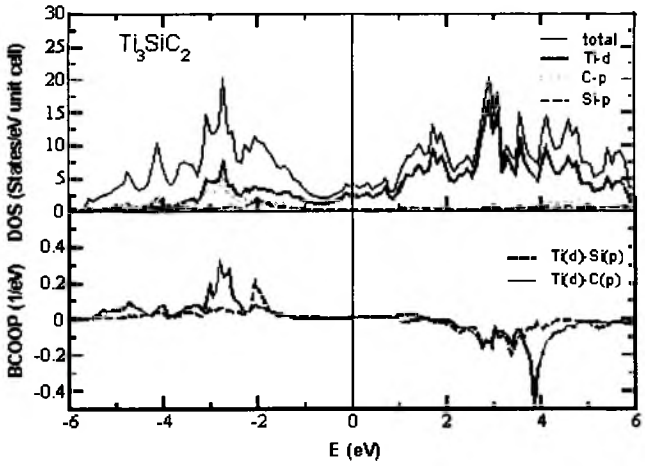

FIG. 13. (Color online) Partial and total density of state (DOS) for Ti_3SiC_2(upper). Balanced crystal orbital overlap population (BCOOP) for Ti_3SiC_2 between Ti *d* and Si *p* orbitals and Ti *d* and C *p* orbitals (lower).

positioned at ~−10 eV, originate from the C 2*s* states, Si 3*s* states contribute to the states between −9 to −6 eV. The states just below the Fermi level (E_F) (−6–0 eV) are dominated by hybridising Ti 3*d* orbitals and C 2*p* states, as are the states above E_F. To analyze the nature of the chemical bonding further, the balanced crystal orbital overlap population (BCOOP) between the Ti *d* and Si *p* orbitals and the Ti *d* and C *p* orbitals was calculated for Ti_3SiC_2 and is shown in Fig. 13.[35] As discussed in Ref. 36 the BCOOP is a function that is positive for bonding hybrid states and negative for antibonding states. A BCOOP analysis will distinguish bonding from antibonding hybrids between any orbitals, e.g., the Ti *d* and C *p* states or the Ti *d* and Si *p* states of the presently discussed materials. From the figure it can be seen that E_F indeed separates the low lying bonding states from the antibonding states above E_F, since the BCOOP is positive for the states below E_F and negative above. Although it has been pointed out that it is hard to compare the strength of a chemical bond, just by inspection of the BCOOP, it should be possible to compare the strength of two similar chemical bonds (e.g., covalent *p*-*d* bonds) from the BCOOP curve. It can be seen in Fig. 13 that the Ti *d*-C *p* overlap is more prominent with higher positive values for the states below E_F than the Ti *d*-Si *p* overlap. This implies that the Ti *d*-C *p* bond are stronger than the Ti *d*-Si *p* bond.

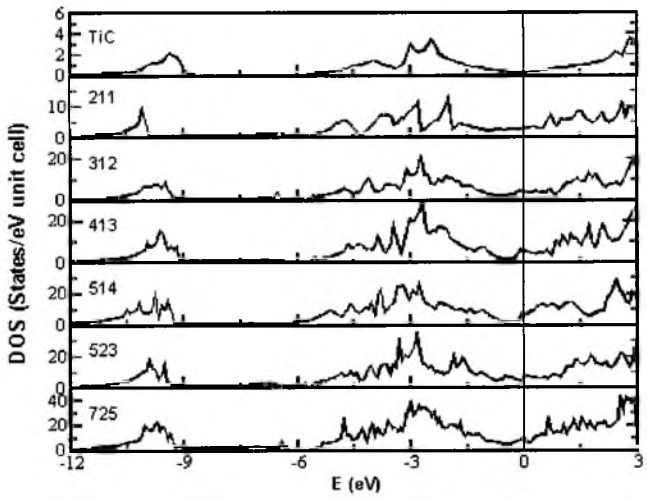

FIG. 12. Total density of state (DOS) for Ti_2SiC, Ti_3SiC_2, Ti_4SiC_3, Ti_5SiC_4 $Ti_5Si_2C_3$, and $Ti_7Si_2C_5$ phases, the Fermi level (E_F) is set at zero energy.

The density of states at Fermi level $N(E_F)$ is, in the simplest approximation, directly related to the electrical conductivity. Our calculated $N(E_F)$ for 211, 312, 413, and 514 phases are 0.36, 0.33, 0.29, and 0.25 states/eV per atom, respectively. This can be compared to TiC, which has a pseudogap at the Fermi level with $N(E_F)$ close to 0.1 states/eV per atom, showing only weak metallic behavior. A trend of decreasing $N(E_F)$ in the sequence of 211, 312, 413, and 514 compounds can be observed, showing decreasing metallicity of the *MAX* phase with increasing number of *n*. A calculated $N(E_F)$=3.96 states/eV per unit cell in 312 is in very good agreement with experimental data of 4.42 states/eV per unit cell derived from heat capacity data.[37]

V. DISCUSSION

A. Phase stability

We have demonstrated that an up to now unknown *MAX* phase, Ti_4SiC_3, can be synthesised as thin films. Previous results for the relative easiness to deposit Ti_3SiC_2 single-crystal films[19] are also reinforced by the present triple-target (elemental) magnetron sputtering technique. Films containing Ti_2SiC could not be deposited. Neither was it possible to synthesise *MAX* phases with $n>4$, i.e., Ti_5SiC_4 or higher. However, two more previously unreported compounds, $Ti_5Si_2C_3$ and $Ti_7Si_2C_5$ have been synthesized. This corresponds to $M_5A_2X_3$ and $M_7A_2X_5$, i.e., a doubled unit cell of $M_{n+1}AX_n$ for n=1.5 and 2.5, respectively. These two are rep-

resentatives of a completely previously unknown type of stacking sequence for the *MAX* phase compounds. The structure can be described as an intergrowth of two known *MAX* structures (e.g., 211 and 312 or 312 and 413) and can be viewed as alternately stacking of 2 and 3, respectively, 3 and 4 *MX* layers between each *A* layer. It was previously assumed that Ti_3SiC_2 was the only $Ti_{n+1}SiC_n$ *MAX* phase.[1] However, our results show that this is not the case and further, there exists more complex *MAX*-phase structures.

To investigate the stability and electronic structure of these novel *MAX* phases in the Ti-Si-C system a series of DFT calculations were carried out. From Table II it can be seen that the correlations between experimental and calculated cell parameters are in agreement. They also fit well with the predicted *c*-axis estimated from d_C and d_{Si} distances (see Fig. 1 and Table II). The DFT calculations give the cohesive energy of a phase, which can be used to estimate the phase stability. The cohesive energy of the *MAX* phase was compared to corresponding cohesive energies for competing phases, given in the phase diagram in Fig. 2. Ti_2SiC and Ti_4SiC_3 have a cohesive energy that is lower than the competing phases and should be stable. In contrast, Ti_5SiC_4 and also the $Ti_5Si_2C_3$ and $Ti_7Si_2C_5$ phases, have much higher cohesive energy than their competing phases, suggesting that these phases are thermodynamically unstable. In reality, the stabilities of the *MAX* phases depend on the sign of ΔG in an assumed reaction where the *MAX* phase decomposes into the competing phases. In principle, the DFT calculations only give the enthalpy change (ΔH) at 0 K for this reaction. Accurate conclusions about phase stabilities at higher temperatures require the knowledge of the temperature dependencies of the enthalpy values and, in addition, entropy effects have to be included. This has not been carried out in this study and we can therefore not draw any final conclusions about the relative stabilities of the new phases at elevated temperatures. However, it is clear that the calculated energy differences between the *MAX* phases and the competing phases are very small. This suggests that these phases should be possible to synthesize as stable or metastable compounds at favorable experimental conditions. In particular, this should be true for low-temperature thin film processes where kinetic constraints play an important role.

It should be noted that 413 was commonly observed in many films and seem relatively easy to grow. In contrast, no successful deposition of the 211 phase was made despite the calculations that suggest that 211 could be stable or at least not very unstable. However, in the phase diagram, 413 lies on the tie line between 312 and TiC, which is a simply balanced system. In contrast, 211 is found in a three-phase region of 312, $TiSi_2$ and Ti_5Si_3, where the last should be considered as $Ti_5Si_3C_x$. However, the calculated energy difference is based on the Ti_5Si_3 without C incorporation. It is likely that the energy difference ΔE would change sign if the calculations had been made for $Ti_5Si_3C_x$ since C is reported to stabilize the Ti_5Si_3 phase.[26,38,39] $Ti_5Si_3C_x$ was commonly observed in Si-rich films and the formation of this silicide when the relative amount of Si increases could effectively hinder the formation of the 211 phase. The observation of 523 is important, however, since its structure contains layers of 211 stacking and thus precludes the possibility for a 211 Ti-Si-C *MAX* phase.

B. Influence of number of Si layers per Ti layer

Our results clearly suggest a relationship between the properties of the *MAX* phases and the number of Si layers per Ti layer. The major difference between a *MAX* phase and TiC is that a C layer in the TiC structure has been exchanged with a Si layer. The two TiC slabs formed on each side of the inserted Si layer are also twinned with the Si layer acting as a mirror plane.[1] The linear relationship in Fig. 10(b) demonstrates that the total energy of a *MAX* phase is directly related to the number of inserted Si layers per Ti layer. Furthermore, the extra energy required to add a Si layer seems to be independent on the distance between the Si layers. This also means that other stacking sequences could be formed. Evidence for this hypothesis is that we have observed random stacking sequences where the system apparently compensates for insufficient amount of Si (or fluctuations in the Si flux during deposition). An example of this is given in the HAADF STEM image in Fig. 7. This observation attests to the ease of altering the stacking sequence of Si layers in the *MAX* film during growth.

It is important to note that the insertion of Si layers in the TiC structure lead to a situation where the Ti atoms will experience different surroundings depending on how closely the Si layers are repeated. In Ti_3SiC_2 two types of Ti positions can be identified, Ti_I and Ti_{II}, where the repeated stacking sequence is Si-Ti_{II}-C-Ti_I-C-Ti_{II}. Both calculations and experimental investigations show that this also affects the Ti-C distance, where Ti_I-C=2.09 Å and Ti_{II}-C=2.18 Å.[5,40] Calculations also show that the Ti_{II} atomic plane has more free charge density distribution than the Ti_I plane.[41] Furthermore, Si is a much larger atom than C. Therefore, the *MAX* phases have a larger volume per atom than pure TiC [see Fig. 10(a)] and the volume depends on the number of Si layers. In addition, the Ti-Si distance in Ti_3SiC_2 is 2.69 Å, which is considerably longer than the ideal Ti-Si covalent bond of 2.54 Å and suggest that the Ti-Si bond is in fact a weak bond.[10] This conclusion is confirmed by the BCOOP results in Fig. 13, which clearly suggest that the Ti *d*-C *p* bond is stronger than the Ti *d*-Si *p* bond. The relatively weak Ti-Si bond also explains the positive slope of the curve in Fig. 10(b). A *MAX* phase where the *M*-*A* bond is stronger than the *M*-*X* bond should give a curve with a negative slope.

Many physical properties of the $Ti_{n+1}SiC_n$ phases can be related to the relative amount of Si layers per Ti layer. As can be seen in Fig. 11 the calculated bulk modulus decreases linearly with the number of Si layers/Ti layer. This softening is a direct consequence of the changes in bonding conditions due to the formation of the weaker Ti-Si bonds. (It should be noted that, the measured value for Young's modulus of the Ti_3SiC_2 film cannot be directly compared with the calculated bulk modulus since they represent different properties.) Unfortunately, it has not yet been possible to perform hardness measurements on the other deposited phases and we can therefore not experimentally verify the calculated results. However, the calculated trend is not surprising, since the $Ti_{n+1}SiC_n$ actually becomes more and more TiC like with increasing number of *n* (i.e., reduced number of inserted Si layer). The *MAX* phases have similar and very specific deformation behavior with kink formation and delamination

properties, which also have been explained by the weak Ti-Si interaction.[27] The defomation behavior of the thin films in this study have been addressed by Molina *et al.*[23]

All $Ti_{n+1}SiC_n$ *MAX*-phase films show excellent conducting properties (see Table II). This is in good agreement with the DFT calculations, which show a relatively large DOS at Fermi level for all these compounds. The electrical conductivity properties of $Ti_{n+1}SiC_n$ should approach TiC with increasing number of Ti layers. TiC has a pseudogap at the Fermi level, with $N(E_F)$ close to 0.1 states/eV per atom, showing weak metallic behavior. Zhou *et al.* suggest that the difference in charge density distribution between Ti_I and Ti_{II} layers indicate that the Ti_{II} layers contribute more to the electrical conductivity than Ti_I layers.[41] Therefore, the number of Ti_{II} layers per unit cell plays an important role in the electrical conductivity. The highest calculated $N(E_F)$ in the $Ti_{n+1}SiC_n$ system suggests that 211 has higher conductivity than the other *MAX* phases, which is also consistent with that it only contains Ti_{II} type. The ratio of Ti_{II}/Ti in one unit cell are 1 (4/4), 0.667 (4/6), 0.5 (4/8), 0.4 (4/10) in the sequence of 211, 312, 413, and 514, suggesting a decrease of the electrical conductivity with increasing number of *n*.

VI. CONCLUDING REMARKS

We have shown that there are at least three more stable or metastable phases in the Ti-Si-C system than previously reported. It is possible to use dc magnetron sputtering technique to synthesize single-crystal and epitaxial *MAX* phase films of (0001)-oriented Ti_3SiC_2 and Ti_4SiC_3. In addition to Ti_4SiC_3, we have observed two previously unknown compounds $Ti_5Si_2C_3$ and $Ti_7Si_2C_5$. These compounds do not follow the general formula $M_{n+1}AX_n$. Still, they belong to the *MAX* phase family since they share the layered structure. Our DFT calculations suggest that the total energy of the observed *MAX* phases are very similar to the total energy of the competing phases as given by the phase diagram. This can explain the fact that these *MAX* phases are formed under kinetically limited deposition conditions at the relatively low temperature of 900 °C and under the influence of epitaxial stabilization.

The DFT calculations show that many properties, such as total energy, volume and bulk modulus of the *MAX* phases in the Ti-Si-C system can be directly related to the number of inserted Si layers per Ti layer. This can be understood from the very weak interaction between Ti and Si compared to Ti and C. This lowers the cohesive energy, which increases the cell volume/atom and softens the *MAX* phase with increasing number of Si layers per Ti layer. Our experimental results suggest that *MAX* phase films with designed electrical and mechanical properties can be synthesised by tuning of the Si content.

Furthermore, we can conclude from the calculations that the insertion of a Si layer cost a certain amount of energy for the structure regardless of how closely the Si layers are packed in the TiC matrix. We have also observed random stacking sequences within the *MAX* phase films. This opens up the prospect for design of artificial and complex *MAX* phase structures, such sequences should be possible to manufacture by careful tuning of the element fluxes during deposition.

Finally, our study shows that previously unknown and previously unknown *MAX* phases can be synthesized using thin films deposition. DFT calculations can be used to predict properties and relative stability of candidate compounds. We suggest that this approach can be used to find *MAX* phases of other elements. This could have large impact in materials development since it is likely that the very useful properties of Ti_3SiC_2 can be improved or surpassed.

ACKNOWLEDGMENTS

The Swedish Strategic Research Foundation (SSF) Materials Research Programs on Low-Temperature Thin Film Synthesis and Fundamental Research and Applications of Magnetism (FRAM), the Swedish Research Council (VR), the Swedish Agency for Innovation System (VINNOVA) Project on Industrialization of *MAX* phase coatings, the Magnus Bergwalls Stiftelse, the Göran Gustafsson foundation and the Wenner-Gren Foundation are acknowledged for financial support. Frederick Seitz Materials Research Laboratory at University of Illinois and Dr. J. M. Molina-Aldareguia are acknowledged for contributions to the TEM study.

[1] M. W. Barsoum, Prog. Solid State Chem. **28**, 201 (2000).
[2] V. H. Nowotny, Prog. Solid State Chem. **5**, 27 (1971).
[3] K. Tang and L. Wu, Mater. Lett. **57**, 106 (2002).
[4] W. Jeitschko and H. Nowotny, Monatsch. Chem. **98**, 329 (1966).
[5] Y. Zhou and S. Chen, J. Phys.: Condens. Matter **13**, 10001 (2001).
[6] B. Holm and B. Johansson, J. Appl. Phys. **91**, 9874 (2002).
[7] M. W. Barsoum and T. El-Raghy, Am. Sci. **89**, 334 (2001).
[8] M. W. Barsoum, T . El-Raghy, and L. U. J. T. Ogbuji, J. Electrochem. Soc. **144**, 2508 (1997).
[9] M. W. Barsoum and T. El-Raghy, Metall. Mater. Trans. A **30**, 363 (1999).
[10] M. W. Barsoum, W. D. Porter, H. Wang, E. A. Payzant, and C. R. Hubbard, J. Phys. Chem. Solids **60**, 429 (1999).
[11] M. W. Barsoum, V. Y. Rud, and T. El-Raghy, Phys. Rev. B **62**, 10 194 (2000).
[12] T. El-Raghy, P. Blau, and M. W. Barsoum, Wear **238**, 125 (2000).
[13] I. M. Low, *et al.*, J. Am. Ceram. Soc. **81**, 225 (1998).
[14] S. Myhra, J. W. B. Summers, and E. H. Kisi, Mater. Lett. **39**, 6 (1999).
[15] M. W. Barsoum, T. El-Raghy, and M. Radovic, Interceram **49**, 226 (2000).
[16] W. J. J. Wakelkamp, F. J. J. van Loo, and R. Metselaar, J. Eur. Ceram. Soc. **8**, 135 (1991).
[17] M. W. Barsoum and T. El-Raghy, J. Am. Ceram. Soc. **79**, 1953 (1996).

[18] J. J. Nickl, K. K. Schweitzer, and P. Luxenberg, J. Less-Common Met. **26**, 335 (1972).
[19] J.-P. Palmquist, P. O. A. Persson, J. Birch, L. Hultman, and P. Isberg, Appl. Phys. Lett. **81**, 835 (2002).
[20] T. Seppänen *et al.*, in *SCANDEM* (Tampere, Finland, 2002).
[21] J. Emmerlich *et al.*, J. Appl. Phys. (to be published).
[22] W. C. Oliver and G. M. Pharr, J. Mater. Res. **7**, 1564 (1992).
[23] J. M. Molina-Aldareguia, U. Jansson, and L. Hultman, Scr. Mater. **49**, 155 (2003).
[24] R. Yu, L. L. He, and H. Q. Ye, Acta Mater. **51**, 2477 (2003).
[25] R. Yu, Y. C. Zhou, and H. Q. Ye, Acta Mater. **50**, 4127 (2002).
[26] A. J. Thom, V. G. Young, and M. Akinc, J. Alloys Compd. **296**, 59 (2000).
[27] B. J. Kooi, J. Th. M. De Hosson, and M. W. Barsoum, Acta Mater. **51**, 2859 (2003).
[28] P. E. Blöchl, Phys. Rev. B **50**, 17 953 (1994).
[29] G. Kresse and D. Joubert, Phys. Rev. B **59**, 1758 (1999).
[30] D. M. Ceperley and B. J. Alder, Phys. Rev. Lett. **45**, 566 (1980).
[31] J. P. Perdew and A. Zunger, Phys. Rev. B **23**, 5048 (1981).
[32] H. J. Monkhorst and J. D. Pack, Phys. Rev. B 13 (1976).
[33] P. E. Blöchl, O. Jepsen, and O. K. Andersen, Phys. Rev. B **49**, 16 223 (1994).
[34] S. Li *et al.* (unpublished).
[35] A. Grechnev (unpublished).
[36] A. Grechnev, R. Ahuja, and O. Eriksson, J. Phys.: Condens. Matter (to be published).
[37] J. C. Ho and T. El-Raghy, J. Appl. Phys. **85**, 7970 (1999).
[38] J. J. Williams, K. M. Ho, L. Hong, C. L. Fu, and S. K. Malik, Intermetallics **8**, 937 (2000).
[39] J. D. Corbett *et al.*, Chem. Mater. **10**, 2824 (1998).
[40] E. H. Kisi and M. W. Barsoum, J. Phys. Chem. Solids **59**, 1437 (1998).
[41] Y. Zhou and Z. Sun, J. Phys.: Condens. Matter **12**, L457 (2000).